Impact of misfit relaxation and *a*-domain formation on the electrical properties of tetragonal PbZr$_{0.4}$Ti$_{0.6}$O$_3$/PbZr$_{0.2}$Ti$_{0.8}$O$_3$ thin film heterostructures: Experiment and theoretical approach

Ludwig Feigl,[a] I. B. Misirlioglu,[b] Ionela Vrejoiu, Marin Alexe, and Dietrich Hesse
Max Planck Institute of Microstructure Physics, Weinberg 2, D-06120 Halle, Germany

Heterostructures consisting of PbZr$_{0.2}$Ti$_{0.8}$O$_3$ and PbZr$_{0.4}$Ti$_{0.6}$O$_3$ epitaxial films on a SrTiO$_3$ (100) substrate with a SrRuO$_3$ bottom electrode were prepared by pulsed laser deposition. By using the additional interface provided by the ferroelectric bilayer structure and changing the sequence of the layers, the content of dislocations and elastic domain types was varied in a controlled manner. The resulting microstructure was investigated by transmission electron microscopy. Macroscopic ferroelectric measurements have shown a large impact of the formation of dislocations and 90° domain walls on the ferroelectric polarization and dielectric constant. A thermodynamic analysis using the Landau–Ginzburg–Devonshire approach that takes into account the ratio of the thicknesses of the two ferroelectric layers and electrostatic coupling is used to shed light on the experimental data. © *2009 American Institute of Physics*. [DOI: 10.1063/1.3056164]

I. INTRODUCTION

Ferroelectric thin films are in the focus of extensive research for applications[1–4] including but not limited to capacitors, pyroelectric sensors, FeRAMs, and valves for ink, fuel, or medicines. These materials have also stimulated intense scientific debate among the condensed matter community owing to the nonconventional (compared to bulk material) physical properties they possess. One of the main challenges that have been faced during the course of the research devoted to ferroelectrics have been size-related phenomena. In order to integrate ferroelectrics into suitable devices, miniaturization is essential. At certain critical size, strains occurring at interfaces become important,[5] enabling strain engineering of the ferroelectric properties,[6] e.g., by tailoring growth on different substrates.[7] Depending on the preferred substrate-film combination, either compressive or tensile strains can be introduced, the latter being able to tilt the polarization vector from the out-of-plane to the in-plane direction.[8] Another prominent characteristic of electric polarization is the possibility to enhance it to higher values than these measured in bulk via strain-polarization electrostrictive coupling,[9] even though this is not always as extensive as expected.[10–13] Thus, ferroelectric films can be tuned to exhibit either polarization values superior to the corresponding bulk material or an outstanding dielectric constant. Other properties such as the pyroelectric effect are affected as well.[14–16]

However these considerations only hold true for a very confined thickness range. If a critical thickness is exceeded during film growth, the heteroepitaxial film usually starts to relax by forming misfit dislocations, that is accompanied by threading dislocation formation.[17–22] Additional stresses could also arise upon cooling down the film from growth

temperature to room temperature due to different thermal expansion coefficients between film and substrate. For particular ferroelectric films, *a*-domains can form below the Curie temperature (T_C) to further relax the residual stresses.[23,24] These *a*-domains are characterized by their polarization axes lying in the plane of the film-substrate interface. Due to the different elastic strain states they exhibit, they are detectable in electron diffraction. While these relaxation mechanisms could give rise to global and local strain relaxation in the film, they can be detrimental for the ferroelectric behavior.[25] The reason for the latter is that local strain variations induce a position dependent polarization owing to the electrostrictive nature of these systems. Strong internal electric fields due to polarization gradients could develop, smearing out the phase transition, and even suppressing ferroelectricity. Such formations must be avoided in design of ferroelectric components for various applications. One approach to tune the properties by minimizing the aforementioned effects is to grow bilayers or superlattices which combine ferroelectrics with other classes of material, e.g., semi-[26] or superconductors.[27] This way of fabricating structures also allows a precise strain and microstructure control by choosing the appropriate components comprising the functional system. By combining materials with very similar crystallographic properties such as ferroelectric PbTiO$_3$ and paraelectric SrTiO$_3$ (STO) intriguing effects such as very high dielectric constants for a critical thickness ratio are predicted.[28] On the other hand, the presence of such a high dielectric anomaly due to the transition of the ferroelectric layer to the paraelectric phase at a critical fraction of the paraelectric layer is now under debate. Some recent studies[29–31] demonstrate that this critical fraction can be perceived as the point at which the ferroelectric layer can no longer exist in the single-domain state but it will split into 180° electrical domains, equivalent to a thermodynamically more stable phase. Therefore an intrinsic dielectric anomaly will not be exhibited.

[a] Electronic mail: lfeigl@mpi-halle.de.
[b] Present address: Sabancı University, Faculty of Engineering and Natural Sciences, Tuzla/Orhanlı 34956 Istanbul, Turkey.

In this study, fabricated bilayer heterostructures consisting of two tetragonal Pb(Zr,Ti)O$_3$ (PZT) compositions PbZr$_{0.2}$Ti$_{0.8}$O$_3$ (PZT20/80) and PbZr$_{0.4}$Ti$_{0.6}$O$_3$ (PZT40/60) are discussed. The influence of the interface between the ferroelectric layers on the resulting macroscopic electric properties, together with the resulting strains, dislocation states, and domains are investigated. Experimental film growth, microstructural, and electrical characterizations are followed by a Landau–Ginzburg–Devonshire (LGD) approach to interpret the results and to shed light on the impact of *a*-domains on such bilayer structures. It is shown that *a*-domains in bilayers and superlattices can arise under certain strain conditions and can significantly alter the electrical properties. The strain states in the layers can be adjusted by changing the sequence of layer growth or by choosing particular thickness ratios and thicknesses of the layers.

II. EXPERIMENTAL

Pulsed laser deposition (PLD) was used to grow thin film heterostructures on vicinal (100) STO single crystals with a miscut of about 0.1° (CrysTec, Berlin/Germany). TiO$_2$-terminated surfaces with atomically smooth terraces were obtained by etching the STO substrate in buffered hydrofluoric acid[32] and subsequently annealing at 1100 °C for 1 h.[33] The ferroelectric PZT20/80 / PZT40/60 bilayers were successively grown on top of the SrRuO$_3$ (SRO) bottom electrode, which was deposited first on STO (100) in step-flow growth mode.[34] A substrate temperature range of 575–700 °C, an oxygen pressure of 14–30 Pa, a laser fluence of 2.5–5 J/cm^2 and a repetition rate of 5 Hz were used. Circular Pt top electrodes with a diameter of about 100 μm were deposited at room temperature by rf sputtering through a corresponding stencil. Macroscopic characterization comprised ferroelectric hysteresis curves recorded at 1 kHz (AixxACT TF Analyzer) and capacitance-voltage characteristics measured at 100 kHz with a probing voltage of 0.1 V (HP4194A impedance analyzer). The values at 0 V have been used to calculate the equivalent dielectric permittivity using the simple plan-parallel capacitor model. Structure analysis was performed by transmission electron microscopy on cross-section samples employing a Philips CM20T electron microscope at 200 keV primary electron energy, using the STO [010] direction as the one of the incident beam. Piezoresponse force microscopy (PFM) was performed using a scanning probe microscope (ThermoMicroscopes) equipped with a PtIr coated tip (ATEC-EFM-20) with an elastic constant of about 2.8 N m^{-1}.

III. APPROACH AND METHODOLOGY

For a given film-substrate combination with a corresponding lattice misfit, the dislocation content and domain formation in single-composition thin films are determined mainly by the film thickness and the growth conditions. A bilayer structure offers the possibility to control the formation of both features via the presence of the additional interface. Due to the different misfits between the layers and between the individual layers and the substrate, various relaxation and elastic domain states are possible.
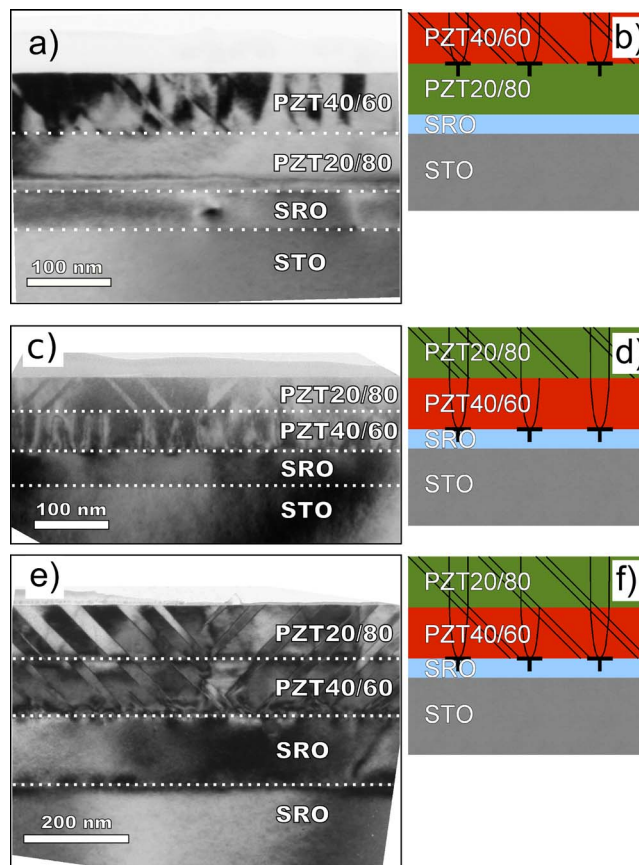

FIG. 1. (Color online) TEM cross-section micrographs [(a), (c), and (e)] and according schemes [(b), (d), and (f)] of ferroelectric bilayers consisting of PZT20/80 and PZT40/60 grown with a SRO bottom electrode on (001)-oriented STO, seen from the [010] STO direction.

In this study, STO substrates were chosen for the growth of *c*-axis oriented PZT20/80 and PZT40/60 layers because of the relatively small lattice misfit such a system would possess. In spite of the latter statement, we were able to introduce elastic *a*-domains into the layers via changing the sequence of the layers where the relaxation sequence of one layer alters the strain state of the other. At growth temperature, PZT20/80 and PZT40/60 have a misfit with the STO substrate of *f*=−1.8% and *f*=−3.0%, respectively. In all present experiments a SRO film was used as bottom electrode. SRO has a misfit of *f*=−0.4%. Its pseudomorphic growth onto STO(100) vicinal crystals was shown experimentally until a thickness of ~75 nm.[22] Therefore, the PZT layers directly experience the misfit with the thick STO substrate.

For PZT layers well above the critical thickness for misfit dislocation formation, there are two main possibilities shown schematically in Fig. 1. (i) When the first grown layer is PZT20/80, this is strained to the substrate with minimal dislocation density due to its small misfit with the SRO/STO; however, the subsequent PZT40/60 layer grows by forming misfit dislocations (MDs) at the interface accompanied by threading dislocations (TDs) propagating to the top surface. In addition, the top layer exhibits narrow *a*-domains which are also terminated at the interface. Transmission electron microscopy (TEM) pictures depicting this case are shown in Fig. 1(a) together with a schematic drawing in Fig. 1(b). (ii)
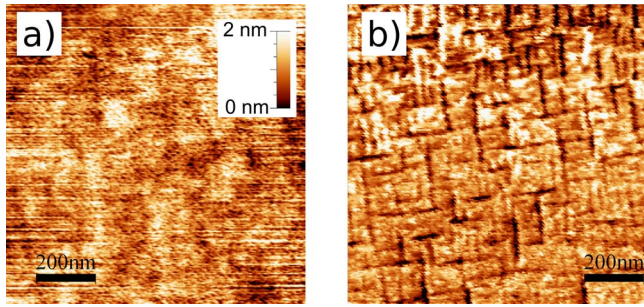
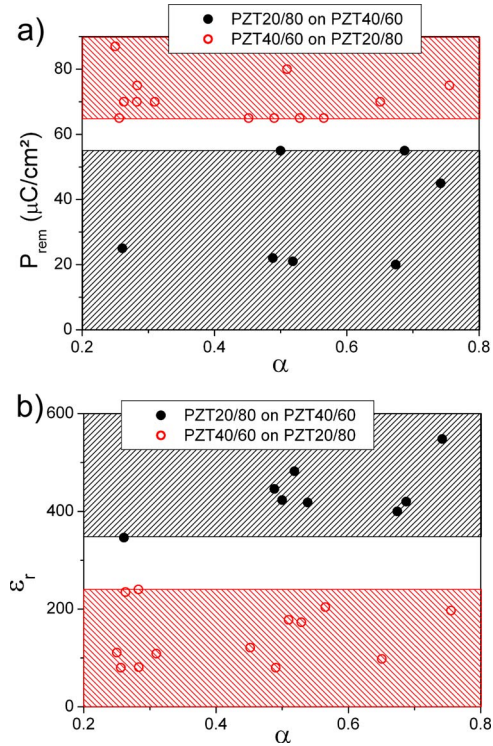FIG. 2. (Color online) (a) Topography and (b) PFM amplitude of the heterostructure shown in Fig. 1(c).

FIG. 3. (Color online) Remnant polarization (a) and dielectric constant (b) of bilayers with a PZT20/80 (○) and a PZT40/60 bottom layer (●) in dependence on the relative thickness. The shaded areas designate the codomains of the measured values caused by the different layer sequences.

When PZT40/60 is used as the bottom layer, quite high densities of MDs form at the interface with the SRO electrode from where many TDs emanate toward the free surface of the structure, thereby crossing the entire PZT20/80 top layer. On the other hand, the abrupt strain state change at the interface could also act as a barrier for the TDs' propagation,[35,36] and somewhat reduces the dislocation content in the top layer with respect to the bottom one. Moreover, two different domain states are possible in the case of this particular dislocation distribution: (1) the a/c-domains are confined to the PZT20/80 layer and terminate at the interface, as shown in Figs. 1(c) and 1(d); (2) the domains are crossing the interface and penetrate through the entire film [Figs. 1(e) and 1(f)] in order to reduce the overall elastic energy of the structure, when the elastic energy of the partially strained film is high enough (possible in thicker films). We would like to point out here that it is one of our motivations to characterize the impact of a-domains on the electrical properties of a bilayer by changing the growth parameters in a controlled manner. Scanning probe investigations of the heterostructures shown in Fig. 1(c) revealed a smooth surface [Fig. 2(a)] and the typical rectangular a-domain pattern visible in the PFM amplitude [Fig. 2(b)].

The dependence of the remnant polarization P_r and dielectric constant ε_r on the relative thickness $\alpha = t_{\mathrm{PZT40/60}}/t_{\mathrm{bilayer}}$, with $t_{\mathrm{bilayer}} = t_{\mathrm{PZT40/60}} + t_{\mathrm{PZT20/80}}$, of the structures are shown in Fig. 3. It can be seen that the different microstructures significantly modify the values of measured P_r and ε_r. Structures with a PZT20/80 bottom layer containing a rather low density of dislocations [Figs. 1(a) and 1(b) and corresponding open circles in Fig. 3] exhibit mean values of $P_r \approx 70$ μC/cm^2 and $\varepsilon_r \approx 145$. In contrast to this picture, the films with a dislocation-rich PZT40/60 bottom layer [Figs. 1(c) and 1(f) and corresponding full circles in Fig. 3] show a smaller P_r of about 35 μC/cm^2 and a much higher $\varepsilon_r \approx 435$. The codomains caused by the two possible sequences in the bilayers are indicated by the shaded areas in Fig. 3.

To explain these experimental observations, we adopted the LGD theory for ferroelectrics to understand the impact of possible influences such as misfit of the layers and electrostatic coupling due to the polarization jump at the interfaces. So, our approach includes appropriate modifications to the bulk LGD potential of the components taking into account the misfit strain due to the film-substrate lattice mismatch, relaxation by dislocations and a-domains as well as the elec-

trostatic coupling of the ferroelectric layers. As the layers are well above the usual thickness for similar systems where interface- and size-effect related phenomena have been reported, such effects have been neglected. We define the free energy density of a bilayer as[28]

$$F = \alpha F_1 + (1 - \alpha)F_2 + F_C, \tag{1}$$

with α being the relative thickness of the layer 1 and F_i ($i=1,2$) being the LGD potential of the individual layers that also contains the elastic energy due to misfit strain. An additional contribution F_c represents the energy due to the electrostatic coupling between the layers as a result of the polarization discontinuity at the interfaces. The free energy densities, F_i, of each layer can be written in the form

$$F_i = F_0 + aP^2 + bP^4 + cP^6 - EP, \tag{2}$$

where a and b are the strain-modified thermodynamic coefficients, c is the higher order dielectric stiffness coefficient in bulk state of layer i, (α_{111} in Ref. 37), P the polarization and E the external electric field parallel to the polarization. Coefficients a and b include the effect of the pseudocubic misfit and the elastic clamping of the thin film to the substrate originating from the addition of elastic energy terms to the bulk free energy. In the presence of different domain states, forms of the coefficients a and b are modified to reflect the presence of domains with different elastic strain values due to the misfit f_i.[38] For the case of a single film consisting of only c-domains,

$$a = \frac{T - T_C}{2\varepsilon_0 C} - f\frac{2Q_{12}}{S_{11} + S_{12}}; \quad b = \alpha_{11} + \frac{Q_{12}^2}{S_{11} + S_{12}}, \tag{3}$$

with T_C being the Curie temperature, C is the Curie constant, S_{ij} is the elastic compliances, Q_{ij} is the electrostrictive coefficients, and α_{11} the dielectric stiffness for the bulk. The coefficients for a single-composition structure consisting of a/c- and a_1/a_2-domains are

$$a^* = \frac{T - T_C}{2\varepsilon_0 C} - f\frac{Q_{12}}{S_{11}}; \quad b^* = \alpha_{11} + \frac{Q_{12}^2}{2S_{11}} \tag{4}$$

for the a/c structure and

$$a^{**} = \frac{T - T_C}{2\varepsilon_0 C} - f\frac{Q_{11} + Q_{12}}{S_{11} + S_{12}},$$

$$b^{**} = \alpha_{11} + \frac{(Q_{11} + Q_{12})^2}{4(S_{11} + S_{12})}, \tag{5}$$

for the a_1/a_2 structure, respectively (here subscript 1 and 2 imply the domain orientations in a layer). In order to find out which domain configuration is stable for a given misfit strain, the free energy has to be implemented with the term describing the purely elastic misfit strain energy, which excludes the self-strain energy. This term is

$$\frac{f^2}{S_{11} + S_{22}} \quad \text{and} \quad \frac{f^2}{2S_{11}}, \tag{6}$$

for the single c-domain state and the a_1/a_2-domain configuration and for the a/c-domain configuration, respectively. Equations (2)–(6) hold only for a single layer at a particular strain state. The minimization of the free energy with respect to polarization and a-domain fraction will give the stable domain configuration at a given temperature. An important term in the free energy of the ferroelectric multilayer heterostructures is the one describing the electrostatic coupling between the component layers. This term should be expected to contribute significantly to the free energy of the system due to the polarization difference at the interface. It must also be kept in mind that the formation of a-domains is not related to any electrostatic interaction but is purely due to elastic misfit strain. The fraction of these a-domains, however, can slightly shift with external applied field that is one of our considerations in this study.

If sufficient elastic strain exists to stabilize c-domains in both layers, the electrostatic coupling term due to the polarization-induced bound charge at the bilayer interface reads

$$F_C = \frac{1}{2\varepsilon_o}\alpha(1 - \alpha)(P_1 - P_2)^2, \tag{7}$$

with ε_0 being the dielectric permittivity of vacuum, P_1 the polarization of the top layer (layer 1), and P_2 the polarization of the bottom layer (layer 2). In the case of elastic strain that favors an a/c-domain configuration of the top layer, the fraction Φ_a of a-domains will be determined by

$$\Phi_a = \frac{(S_{11} - S_{12})(f - Q_{12}P_{c1}^2)}{S_{11}(Q_{11} - Q_{12})P_{c1}^2}. \tag{8}$$

Our approach assumes that the a-domains have an induced c-polarization due to the presence of an uncompensated charge at the interface between the layers. Thus, the single c-domain state of the bottom layer induces a c-component (out of plane) of the polarization in a-domains of the top layer and couples to the c-domain polarization as in Eq. (7). This is due to the susceptibility of the a-domains along the out-of-plane direction with respect to the interface between the layers. Therefore the electrostatic coupling can be described as

$$F_C = \frac{1}{2\varepsilon_0}\alpha(1 - \alpha)((1 - \phi_a)P_{c1} + \phi_a P_{a1} - P_2)^2. \tag{9}$$

Here P_{c1} is the polarization of the c-domains in layer 1 and P_{a1} is the induced out-of-plane polarization in the a-domains of layer 1. Equation (9) simply dictates that the electrostatic coupling will occur between all layers with the contribution from the a-domains. For instance, had there been only a_1/a_2-domain configuration of the top layer, there would have been only induced polarization in layer 1 and the coupling term would be written as

$$F_C = \frac{1}{2\varepsilon_0}\alpha(1 - \alpha)(P_{a1} - P_2)^2. \tag{10}$$

If both layers exhibit an a/c-domain structure the coupling term becomes

$$F_C = \frac{1}{2\varepsilon_0}\alpha(1 - \alpha)((1 - \phi_{a1})P_{c1} + \phi_{a1}P_{a1} - (1 - \phi_{a2})P_{c2}$$
$$- \phi_{a2}P_{a2})^2, \tag{11}$$

with Φ_{a1} and Φ_{a2} the fraction of a-domains in the first and the second layer, respectively. It should be noted here that our method does not take into account spatial variations in polarizations neither in the vicinity of the a-domain/c-domain nor a-domain/a-domain junctions of the two layers but only the sum of polarization values of each layer. The induced c-polarization in the a-domains gives rise to an additional energy term that also has to be taken into account. This can be deduced for each layer where an a-domain has an additional c-polarization component, modifying the free energy of a-domains in a layer i, F_i^a, in the form[39]

$$F_i^a(P, E = 0) = 2a^{**}P_a^2 + aP_c^2 + b_1P_a^4 + bP_c^4 + b_2P_a^2P_c^2$$
$$+ \alpha_{111}(2P_a^6 + P_c^6) + \alpha_{112}(2P_a^4(P_a^2 + P_c^2)$$
$$+ 2P_c^4P_a^2) + \alpha_{123}P_a^4P_c^2, \tag{12}$$

containing the higher order dielectric stiffness coefficients α_{ijk} and the modified coefficients

$$b_1 = 2\left(\alpha_{11} + \frac{1}{2}\frac{(Q_{11}^2 + Q_{12}^2)S_{11} - 2Q_{11}Q_{12}S_{12}}{S_{11}^2 - S_{12}^2}\right)$$
$$+ \left(\alpha_{12} - \frac{(Q_{11}^2 + Q_{12}^2)S_{12} - 2Q_{11}Q_{12}S_{11}}{S_{11}^2 - S_{12}^2} + \frac{Q_{44}^2}{2S_{44}}\right) \quad (13)$$

and

$$b_2 = 2\left(\alpha_{12} + \frac{Q_{12}(Q_{11} + Q_{12})}{S_{11} + S_{12}}\right) \quad (14)$$

for a layer *i*. Depending on the type of elastic strain states in the layers and relaxation mechanisms, the stable equilibrium domain configuration in our bilayers can be determined using relations (1)–(14). *F* has to be minimized with respect to each polarization component in order to calculate the polarizations in each layer. It is important to remind here that the polarization solutions of both layers, including the solutions for the *a*-domains are all connected through the electrostatic coupling. Following the polarization solutions, we also calculated the small signal dielectric constant, ε_r, which is basically the polarization difference arising in the structure when applying a small external electric field E_0:

$$\varepsilon_r = \frac{P(E = E_0) - P(E = 0)}{E_0}. \quad (15)$$

We now apply our methodology to the cases that resemble the experimentally observed data. For the structures shown in Figs. 1(a)–1(d) the model is assumed to include a single-domain bottom layer and a multidomain top layer. In order to compare the measured values (given by the dots in Fig. 3) with these obtained via the theoretical approach, the self-strain free pseudocubic strain states of the different layers must be known including the domain fractions. Since these are quite difficult to determine experimentally and vary from sample to sample, only the cases that are bordering our experimental data and observed microstructures are considered in the calculations. Such an approach takes into account the misfit relaxation by dislocations in each layer at growth temperature and the developing thermal strain in each layer upon cooling. Thus, *a*-domain formation in any of the layers will result once the particular layer reaches its T_c and if the misfit strain favors an a/c domain pattern of the layer, determined by comparing the free energies of possible domain states. Moreover, there could exist an a_1/a_2 pattern of a layer with the other layer being in any of the a/c-, c-, or a_1/a_2-domain states depending on the individual strain states of the layers.

The first considered case is a bilayer with a fully strained PZT40/60 layer (misfit at room temperature: $f_{RT} = -3.2\%$) on top of a fully strained PZT20/80 layer ($f_{RT} = -2.0\%$). The corresponding values for polarization and dielectric constant are given in Figs. 4(a) and 4(b) by the red dotted line No. 1. However, the TEM image in Fig. 1(a) shows a high density of TDs in the top PZT40/60 layer suggesting a misfit dislocation driven relaxation of the layer. In the extreme case, this layer can be treated as fully relaxed at growth temperature where thermal strains develop upon cooling resulting in small compressive RT misfit of $f_{RT} = -0.1\%$. The results are shown by line No. 2 in Figs. 4(a) and 4(b), where P_r is smaller and ε_r larger compared to line No. 1. In reality, both
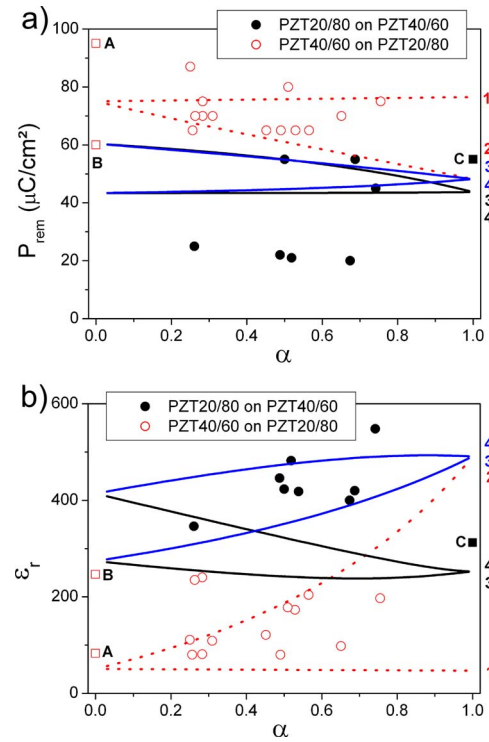

FIG. 4. (Color online) Remnant polarization (a) and dielectric constant (b) of bilayers with a PZT20/80 (○) and a PZT40/60 bottom layer (●) in dependence on the relative thickness. □ and ■ designate single PZT layers consisting of strained PZT20/80 (a), relaxed PZT20/80 (b), and relaxed PZT40/60 (c). The lines display the results of the LGD theory for bilayers with a PZT20/80 bottom layer (red dotted line, 1, 2) and a PZT40/60 bottom layer with (blue continuous line, 3′, 4′) and without a/c domain walls (black continuous line, 3, 4).

layers will partially relax to some point, determined by the PLD growth conditions, which cannot be precisely controlled or exactly measured. It has to be assumed that the measured values lie somewhere in the range between the two calculated red dotted lines. Concerning the PZT20/80 on PZT40/60 bilayer with domains terminated at the interface [Fig. 1(c)], the curves Nos. 3 and 4 (black lines) show the results of a relaxed PZT20/80 ($f_{RT} = -0.1\%$) on a relaxed PZT40/60 ($f_{RT} = -0.1\%$) and of a strained PZT20/80 ($f_{RT} = +1.1\%$) on a relaxed PZT40/60 layer, respectively. In this case, the film containing a strained PZT20/80 layer exhibits a smaller P_r and a larger ε_r. The lines denoted as 3′ and 4′ cover the possibility of domains to propagate through both layers as shown in Fig. 1(e). It can be seen that the influence of the a/c-domain structure on P_r is small while ε_r increases considerably.

IV. RESULTS AND DISCUSSION

Although the properties and lattice constants of the tetragonal PZT compositions PZT20/80 and PZT40/60 are similar, the combination of both in the form of bilayers results in very different values for the remnant polarization P_r and the dielectric constant ε_r when the layer sequence with respect to the substrate is changed. The main reasons for this behavior are (1) the different lattice parameters of the two PZT compositions and (2) the dependence of the misfit strain of the top layer on the relaxation state of the bottom layer.

During the growth on the STO (100) substrate, the lattice constant of PZT20/80 is close enough to allow a coherent growth [reported for films thinner than ~100 nm (Ref. 40)], whereas PZT40/60 forms dislocations to relax the strain caused by its higher lattice mismatch with the substrate. Furthermore, the domain and polarization states of the two layers are not independent from each other due to strain and electrostatic effects. The interface between the ferroelectric layers is the site of the mechanical and electrostatic couplings and it can, therefore, act as a barrier or favor nucleation of domains and dislocations, allowing different domain states and dislocation densities in the two layers. Ferroelectric bilayers containing PZT20/80 as bottom layer, hence with both layers subjected to compressive stress, show high polarization values and a low dielectric constant (curve No. 1 in Fig. 4). The consecutive relaxation of the PZT40/60 (curve No. 2) and of the PZT20/80 layer (curve No. 3) leads to a decrease in P_r and increase in ε_r due to the a-domains and the domain wall contribution.[41] If PZT40/60 is grown as the bottom layer, tensile stresses can develop in the PZT20/80 layer. In this case P_r would further decrease and ε_r further increase (curve No. 4) compared to states with less tensile stress. As it is shown in Fig. 1(e), the domains might also cross the interface. This causes a slight increase in P_r and a significant increase in ε_r (curve Nos. 3′ and 4′) due to the further relaxation and the contributions of the a/c-domain structure compared to the films containing the untwinned PZT40/60 bottom layer.

For the case of α becoming 0 or 1, the structure entirely consists of either PZT20/80 or PZT40/60, respectively. At $\alpha=0$ the values correspond to a PZT20/80 film under compression (curve Nos. 1 and 2) without domains, and twinned films under no stress (curve Nos. 3 and 3′) and tension (curve Nos. 4 and 4′), respectively. On the other hand at $\alpha=1$ the values for a PZT40/60 film subjected to compressive stress (curve No. 1) and no stress with (curve Nos. 2, 3′, and 4′) and without a-domains (curve Nos. 3 and 4) can be read off. These results can be compared to measurement data obtained on single layer films (■ and □ in Fig. 4). It turns out that the P_r value of a relaxed PZT20/80 (designated with B) single layer is in very good accordance with the calculations, whereas the measured P_r value of a strained PZT20/80 layer (A) is much higher. The latter phenomenon has already been observed and reported in a previous work.[41] The computed values for a PZT40/60 layer (C) cover the measured result and indicate a highly but not fully relaxed film. Regarding the values of ε_r, there is a good agreement between simulation and experiment for PZT20/80 and the calculated range includes the measured value for PZT40/60.

Despite the good agreement between the results of our modified LGD approach and the experiment, in general, there are observable deviations of the computed values from real data. These occur because the model used is still quite macroscopic in comparison to the diversity of the features in the investigated system. The major influences considered by the model are the global misfit strain in the layers and the overall electrostatic coupling between the layers. For a complete model, additional effects induced by the interface between the ferroelectric layers and by the interfaces with the metal electrodes should be taken into account. Charged traps can significantly contribute to ε_r.[42] The presence of the "dead layer" at the interfaces may alter the ferroelectric properties[43,44] in addition to possible existence of space charges, which can also change the properties of the bilayer.[45] Misfit dislocations that form at the interface are accompanied by local strains and possible internal fields originating from these microstresses affecting both P_r and ε_r.[25,46,47] These misfit dislocations give rise to threading dislocations as a by-product[15] which could smear out the distribution of P_r rather than a single value.[44,48] Overall, despite the simplicity of the approach, the variations of the experimental observations can be elucidated and the effect of a-domains can be highlighted through the adopted methodology.

V. SUMMARY AND CONCLUSIONS

Different dislocation densities and domain states were induced in PZT20/80 / PZT40/60 bilayers grown on SRO-coated STO (100) by changing the growth sequence and the thickness of the component layers. The macroscopic properties are quite different from those measured in films comprised of individual components. Clearly, such a trend is determined by the extent of relaxation via dislocation formation and elastic domain formation as well as the electrostatic interaction between the layers. A modified LGD approach was used to provide a semiquantitative explanation for this behavior taking into account the misfit strains, the electrostatic coupling, and the formation of an a/c-domain structure. Considering the simplicity of our model the experimental data are well described. The increase in the dielectric constant accompanied by a deterioration of the remnant polarization can be attributed to the changeover from compressive to tensile misfit strain that impacts the Curie points of the layers. Especially, growing the PZT40/60 as the bottom layer drives a rapid relaxation of this bottom layer, imposing a tensile strain state in the upper layer. Then the upper layer experiences a tensile strain that triggers a-domain formation in this layer following relaxation via misfit dislocations. According to our computed results the occurrence of a-domains slows down the decrease in the remnant polarization in the investigated strain range with increasing tensile misfit, while the domain walls give a significant contribution to the dielectric constant. This study demonstrates that functional ferroelectric structures with controlled microstructures can be fabricated via choosing the appropriate sequence of layers and their appropriate thicknesses, allowing for the possibility to tune the strain state of the system.

ACKNOWLEDGMENTS

[1] P. Muralt, J. Micromech. Microeng. **10**, 136 (2000).

[2] N. Setter and R. Waser, Acta Mater. **48**, 151 (2000).

[3] O. Auciello, J. Appl. Phys. **100**, 051614 (2006).

[4] J. F. Scott, Science **315**, 954 (2007).

[5] D. Hesse and M. Alexe, Z. Metallkd. **96**, 448 (2005).

[6] D. G. Schlom, L.-Q. Chen, C.-B. Eom, K. M. Rabe, S. K. Streiffer, and J.-M. Triscone, Annu. Rev. Mater. Res. **37**, 589 (2007).

[7] B. S. Kwak, A. Erbil, J. D. Budai, M. F. Chrisholm, L. A. Boatner, and B. J. Wilkens, Phys. Rev. B **49**, 14865 (1994).

[8] K. Iijima, R. Takayama, Y. Tomita, and I. Ueda, J. Appl. Phys. **60**, 2914 (1986).

[9] R. E. Cohen, Nature (London) **358**, 136 (1992).

[10] C. Ederer and N. A. Spaldin, Phys. Rev. Lett. **95**, 257601 (2005).

[11] C.-L. Jia, V. Nagarajan, J.-Q. He, L. Houben, T. Zhao, R. Ramesh, K. Urban, and R. Waser, Nature Mater. **6**, 64 (2007).

[12] H. N. Lee, S. M. Nakhmanson, M. F. Chisholm, H. M. Christen, K. M. Rabe, and D. Vanderbilt, Phys. Rev. Lett. **98**, 217602 (2007).

[13] C.-L. Jia, S.-B. Mi, K. Urban, I. Vrejoiu, M. Alexe, and D. Hesse, Nature Mater. **7**, 57 (2008).

[14] K. Iijima, Y. Tomita, R. Takayama, and I. Ueda, J. Appl. Phys. **60**, 361 (1986).

[15] Z.-G. Ban and S. P. Alpay, Appl. Phys. Lett. **82**, 3499 (2003).

[16] A. Sharma, Z.-G. Ban, S. P. Alpaya, and J. V. Mantese, J. Appl. Phys. **95**, 3618 (2004).

[17] J. W. Matthews and A. E. Blakeslee, J. Cryst. Growth **27**, 118 (1974).

[18] W. D. Nix, Metall. Trans. A **20**, 2217 (1989).

[19] J. S. Speck and W. Pompe, J. Appl. Phys. **76**, 466 (1994).

[20] S. Stemmer, S. K. Streiffer, F. Ernst, and M. Rühle, Phys. Status Solidi A **147**, 135 (1995).

[21] T. Suzuki, Y. Nishi, and M. Fujimoto, Philos. Mag. A **79**, 2461 (1999).

[22] S. H. Oh and C. G. Park, J. Appl. Phys. **95**, 4691 (2004).

[23] S. P. Alpay and A. L. Roytburd, J. Appl. Phys. **83**, 4714 (1998).

[24] S. P. Alpay, V. Nagarajan, L. A. Bendersky, M. D. Vaudin, S. Aggarwal, R. Ramesh, and A. L. Roytburd, J. Appl. Phys. **85**, 3271 (1999).

[25] M. W. Chu, I. Szafraniak, R. Scholz, C. Harnagea, D. Hesse, M. Alexe, and U. Gosele, Nat. Mater. **3**, 87 (2004).

[26] M. Okuyama, K. Yokoyama, and Y. Hamakawa, Jpn. J. Appl. Phys., Part 1 **18**, 1111 (1979).

[27] C. Bjormander, A. M. Grishin, B. M. Moon, J. Lee, and K. V. Rao, Appl. Phys. Lett. **64**, 3646 (1994).

[28] A. L. Roytburd, S. Zhong, and S. P. Alpay, Appl. Phys. Lett. **87**, 092902 (2005).

[29] F. A. Urtiev, V. G. Kukhar, and N. A. Pertsev, Appl. Phys. Lett. **90**, 252910 (2007).

[30] Y. L. Li, S. Y. Hu, D. Tenne, A. Soukiassian, D. G. Schlom, X. X. Xi, K. J. Choi, C. B. Eom, A. Saxena, T. Lookman, Q. X. Jia, and L. Q. Chen, Appl. Phys. Lett. **91**, 112914 (2007).

[31] A. P. Levanyuk, personal communication (9th February 2007).

[32] M. Kawasaki, K. Takahashi, T. Maeda, R. Tsuchiya, M. Shinohara, O. Ishiyama, T. Yonezawa, M. Yoshimoto, and H. Koinuma, Science **266**, 1540 (1994).

[33] G. Koster, G. Rijnders, D. H. A. Blank, and H. Rogalla, Physica C **339**, 215 (2000).

[34] W. Hong, H. N. Lee, M. Yoon, H. M. Christen, D. H. Lowndes, Z. G. Suo, and Z. Y. Zhang, Phys. Rev. Lett. **95**, 095501 (2005).

[35] H. Amano, M. Iwaya, N. Hayashi, T. Kashima, M. Katsuragawa, T. Takeuchi, C. Wetzel, and I. Akasaki, MRS Internet J. Nitride Semicond. Res. **4**, G10.1 (1999).

[36] A. Dadgar, M. Poschenrieder, O. Contreras, J. Christen, K. Fehse, J. Blasing, A. Diez, F. Schulze, T. Riemann, F. A. Ponce, and A. Krost, Phys. Status Solidi A **192**, 308 (2002).

[37] N. A. Pertsev, A. G. Zembilgotov, and A. K. Tagantsev, Phys. Rev. Lett. **80**, 1988 (1998).

[38] V. G. Koukhar, N. A. Pertsev, and R. Waser, Phys. Rev. B **64**, 214103 (2001).

[39] N. A. Pertsev, V. G. Koukhar, H. Kohlstedt, and R. Waser, Phys. Rev. B **67**, 054107 (2003).

[40] I. Vrejoiu, G. Le Rhun, L. Pintilie, D. Hesse, M. Alexe, and U. Goesele, Adv. Mater. (Weinheim, Ger.) **18**, 1657 (2006).

[41] G. Le Rhun, I. Vrejoiu, L. Pintilie, D. Hesse, M. Alexe, and U. Goesele, Nanotechnology **17**, 3154 (2006).

[42] L. Pintilie, I. Vrejoiu, D. Hesse, G. Le Rhun, and M. Alexe, Phys. Rev. B **75**, 224113 (2007).

[43] A. M. Bratkovsky and A. P. Levanyuk, Phys. Rev. B **63**, 132103 (2001).

[44] M. Stengel and N. A. Spaldin, Nature (London) **443**, 679 (2006).

[45] I. B. Misirlioglu, M. Alexe, L. Pintilie, and D. Hesse, Appl. Phys. Lett. **91**, 022911 (2007).

[46] S. P. Alpay, I. B. Misirlioglu, V. Nagarajan, and R. Ramesh, Appl. Phys. Lett. **85**, 2044 (2004).

[47] I. B. Misirlioglu, A. L. Vasiliev, M. Aindow, and S. P. Alpay, Integr. Ferroelectr. **71**, 67 (2005).

[48] I. Vrejoiu, G. Le Rhun, N. D. Zakharov, D. Hesse, L. Pintilie, and M. Alexe, Philos. Mag. **86**, 4477 (2006).